Proc. Natl. Acad. Sci. USA
Vol. 95, pp. 12277–12282, October 1998
Biophysics

Temperature dependence of amyloid β-protein fibrillization

YOKO KUSUMOTO†, ALEKSEY LOMAKIN†, DAVID B. TEPLOW‡, AND GEORGE B. BENEDEK†§

†Department of Physics and Center for Materials Science and Engineering, Massachusetts Institute of Technology, Cambridge, MA 02139; and ‡Center for Neurologic Diseases, Brigham and Women's Hospital, Boston, MA 02115

Contributed by George B. Benedek, August 6, 1998

ABSTRACT **Fibrillogenesis of the amyloid β-protein (Aβ) is believed to play a central role in the pathogenesis of Alzheimer's disease. Previous studies of the kinetics of Aβ fibrillogenesis showed that the rate of fibril elongation is proportional to the concentration of monomers. We report here the study of the temperature dependence of the Aβ fibril elongation rate constant, k_e, in 0.1 M HCl. The rate of fibril elongation was measured at Aβ monomer concentrations ranging from 50 to 400 μM and at temperatures from 4°C to 40°C. Over this temperature range, k_e increases by two orders of magnitude. The temperature dependence of k_e follows the Arrhenius law, $k_e = A \exp(-E_A/kT)$. The preexponential factor A and the activation energy E_A are $\approx 6 \times 10^{18}$ liter/(mol·sec) and 23 kcal/mol, respectively. Such a high value of E_A suggests that significant conformational changes are associated with the binding of Aβ monomers to fibril ends.**

Alzheimer's disease (AD) is the most common cause of dementia and the fourth leading cause of death in the United States (1). AD is characterized by the deposition of the 40 to 42-residue amyloid β-protein (Aβ) in the cerebral parenchyma and vasculature and by the formation of intracellular neurofibrillary tangles (2). Two major types of deposit are distinguished, on the basis of the presence or absence of fibrillar Aβ aggregates (2). Those deposits containing fibrillar elements are associated with areas of damaged neuropil, whereas afibrillar deposits are found within otherwise normal tissue (3). *In vitro*, fibrillar forms of Aβ are toxic to neuronal cells (3, 4). The deposition of fibrillar Aβ is thus thought to be a seminal event in the pathogenesis of AD (5). An increasing body of genetic evidence supports this conclusion (6). In particular, mutations that increase the overall production of Aβ, that increase the relative amount of the particularly amyloidogenic 42-residue form of the peptide, or that facilitate Aβ deposition have been found to cause familial forms of AD.

The central role of fibrillar Aβ in AD pathogenesis suggests that therapeutic approaches focused on the fibrillogenesis process would be highly promising. Detailed knowledge of the mechanism of Aβ fibrillogenesis helps to identify specific steps in the fibrillogenesis process to which a drug might be targeted. This knowledge, together with information on the production of Aβ monomers and the kinetics of Aβ fibril degradation, is also needed to foresee the consequences of intervention at a particular stage of fibrillogenesis. These considerations have stimulated active investigations of the kinetics of Aβ fibrillization.

In vitro studies have suggested that Aβ fibrillogenesis occurs in two distinct stages, nucleation and elongation of fibers (7). The nucleation stage is a series of thermodynamically unfavorable steps leading to the creation of a stable nucleus. It is not clear at present how big the nucleus is. The smallest particles detected in the fibrillogenesis process at low pH have sizes that correspond to the diameter of an Aβ fibril (8). This finding is consistent with the view that nuclei are very short fibrils. Heterogeneous nucleation, e.g., on non-Aβ seeds, may also occur, which is a plausible mechanism for the nucleation of Aβ fibrils *in vivo*. *In vitro*, preexisting heterogeneous nuclei or Aβ seeds present a serious experimental problem. The length that fibrils reach when all soluble peptide is exhausted is inversely proportional to the total number of nucleated or preexisting fibrils. In turn, the length of the fibrils is the key parameter that determines the kinetics of fibril-to-fibril aggregation, sedimentation of fibril aggregates, or gelation of the solution. Thus, lack of control of the number of seeds leads to poor reproducibility, both in fibrillogenesis kinetics and in the macroscopic properties of the aggregated Aβ sample.

Elongation of an individual fibril, however, is a well defined process that is insensitive to variation in nucleus or seed concentration. There is significant experimental evidence that the kinetics of the elongation process is of the first order, i.e., Aβ monomers bind to the fibril ends with a rate proportional to their concentration c (8–10):

$$\frac{dN_f}{dt} = k_e c. \qquad [1]$$

Here, N_f is the number of monomers in a fibril. The proportionality coefficient relating the elongation rate dN_f/dt to the concentration of Aβ monomers is termed the elongation rate constant, k_e. For the sake of simplicity, the term "monomer" is used to describe the soluble form of Aβ that adds to fibril ends. It has been assumed in the past that soluble, nonfibrillar Aβ was monomeric; however, the possibility exists that soluble Aβ is actually dimeric (11, 12).

The elongation rate constant is a fundamental characteristic of the fibrillogenesis process. It varies with solution conditions such as pH, ionic strength, and temperature and can be altered by chemical reagents capable of binding to the Aβ monomer itself or to a fibril end. Quantitative determination of the effects of fibrillogenesis conditions on k_e provides valuable leads to understanding the molecular mechanism of fibril elongation.

Several methods have been used to study the kinetics of Aβ fibrillogenesis. The simplest method, turbidimetry, monitors the total light scattering from the sample (13, 14). The intensity of scattered light grows proportionally to the molecular weight of the scattering particles and ideally would reflect fibril elongation. In practice, however, the bulk of the scattering intensity arises from fibril-to-fibril association. The kinetics of fibril association depends on fibril size, concentration, and whether the sample is stirred. These factors make quantitative interpretation of turbidimetry results extremely difficult, if not impossible.

The publication costs of this article were defrayed in part by page charge payment. This article must therefore be hereby marked "*advertisement*" in accordance with 18 U.S.C. §1734 solely to indicate this fact.

Abbreviations: AD, Alzheimer's disease; Aβ, amyloid β-protein; QLS, quasielastic light scattering.

§To whom reprint requests should be addressed at: Department of Physics, Room 13-2005, Massachusetts Institute of Technology, Cambridge, MA 02139. e-mail: benedek@mit.edu.

Naiki *et al.* (9) have used thioflavine T binding to study the kinetics of Aβ fibril elongation. This method measures the total concentration of fibrillar Aβ, which increases at the rate $k_e cN$, where N is number concentration of fibrils. Because N is unknown, it is impossible to determine the value of k_e. However, by comparing samples of identical concentration, seeded with the same number of fibrils, Naiki *et al.* were able to study relative temperature and pH dependencies of k_e (9), as well as the effect of apolipoprotein E on the elongation rate (15).

Quasielastic light scattering (QLS), in contrast, allows the simultaneous, noninvasive monitoring of both size and molecular weight of particles in solution and is particularly well suited for studying protein aggregation phenomena (16). This method has been used successfully to study the late stages of fibrillogenesis and the effect of sample preparation procedures on the fibrillization process (17, 18). The principal difficulty in using QLS is the same as for the less sophisticated turbidimetry method: fibril-to-fibril association can lead to the formation of large aggregates, which dominate the light scattering and complicate data interpretation. In our previous study (8), we discovered that fibrillization of Aβ in 0.1 M HCl is highly reproducible, is free from fibril-to-fibril association, and yields fibrils that are morphologically indistinguishable from those formed *in vivo*. QLS was used to monitor both nucleation and elongation of Aβ fibrils and to determine quantitatively the elongation and nucleation rate constants. These studies led to development of a full mathematical description of the fibrillogenesis process (19). In this publication, we present our study of the temperature dependence of the elongation rate of Aβ fibrils in 0.1 M HCl and report the activation energy required for the binding of Aβ monomers to fibril ends.

MATERIALS AND METHODS

Protein Preparation. Peptide synthesis, purification, and characterization have been described previously (8, 11). Briefly, Aβ(1–40) was made on an automated peptide synthesizer (Applied Biosystems model 430A) by using 9-fluorenylmethoxycarbonyl-based methods. Reverse-phase high-performance liquid chromatography was used for peptide purification. Quantitative amino acid analysis and matrix-assisted laser desorption/ionization time-of-flight mass spectrometry yielded the expected composition and molecular weight. The purified peptide was stored as a lyophilizate at -20°C.

Experimental Protocol. We first conducted experiments to establish that the temperature dependence of elongation rates follows the Arrhenius law. Aβ was dissolved in 0.1 M HCl (pH = 1) at 4°C to a nominal concentration of 250 μM, vortexed gently, and filtered through a 20-nm inorganic membrane filter (Anotop 10 Plus, Whatman) into a QLS cuvette. The sample was then incubated for 4 hr at 25°C. As reported previously (8), at this concentration, Aβ monomers form micelle-like structures that serve as centers of nucleation. The sample was monitored by QLS, and, after 4 hr, when fibrils were $\approx$120 nm long (hydrodynamic radius $R_h \approx 20$ nm), was diluted 5-fold and was aliquotted equally among four new cuvettes. One cuvette was used for monitoring fibrillogenesis at the highest temperature (35°C), while the other three were frozen and kept at -85°C. Preliminary experiments showed no detectable alteration in the course of fibrillogenesis in samples that had been frozen and thawed. After the fibrillization process in the first sample was complete, each of the remaining aliquots was thawed sequentially and the time dependence of fibril size was monitored at 25°C, 15°C, and 4°C. This procedure ensured identical numbers of fibrils as well as identical total Aβ concentration in each aliquot. However, before the incubation at each temperature, there was already considerable elongation of fibrils. Such significant growth diminished the accuracy with which the value of the elongation rate could be measured. To improve this accuracy, we performed a series of experiments in which samples were monitored at different temperatures immediately upon dissolution. Lyophilized peptide was dissolved and filtered as above, then split into halves. The fibrillogenesis in the aliquots was then monitored concurrently in two separate spectrometers held at two different temperatures, typically 4°C and 25°C. Such concurrent measurements of fibrillogenesis at two different temperatures were performed at nominal concentrations of 100, 125, 250, and 375 μM. The 125 μM sample was centrifuged at $20{,}000 \times g$ for 30 min rather than being filtered.

In each experiment, when fibrillogenesis was complete, the total Aβ concentration was determined by amino acid analysis. These final concentrations were less, sometimes significantly less, than the nominal concentration that was calculated from the weight of the initially dissolved material. Part of the loss was likely because of removal of preexistent fibrils and aggregates during filtration. As will become clear in the next section, the uncertainty in the initial concentration of soluble Aβ is insignificant for the estimation of the thermodynamic parameters of the binding reaction between Aβ monomer and fibril end.

QLS and Data Analysis. QLS measurements were performed with a 144-channel Langley Ford model 1097 correlator (Amherst, MA) and a Coherent Innova 90 argon laser (514 nm) (Coherent, Santa Clara, CA). The scattering angle was 90°. The temperature was controlled by using an Endocal bath (Neslab Instruments, Portsmouth, NH) and a temperature control unit with a feedback loop for fine-tuning.

A constrained regularization method was used to determine the mean diffusion coefficient, $\bar{D}$ (20). The mean hydrodynamic radius R_h was calculated by using the Stokes–Einstein relation $\bar{D} = k_B T/6\pi\eta R_h$, where k_B is Boltzmann's constant, T is the absolute temperature, and η is the solvent viscosity. The average fibril length L was then calculated from R_h, assuming that fibrils are stiff rods with diameter 8 nm, using an appropriate interpolation formula (8). Finally, the total number of monomers in the fibril was determined according to $N_f = \lambda L$, where λ is the linear density of Aβ within the fibril ($\lambda = 1.6$ nm^{-1} (17)). By monitoring $\bar{D}$, the temporal evolution of $R_h(t)$ or $N_f(t)$ may thus be determined. The elongation rate $dN_f/dt = k_e c$ was determined from the slope of the initial linear domain of the curve of R_h vs. time.

RESULTS AND DISCUSSION

We formulated previously a theoretical description of Aβ fibrillogenesis at low pH (19). We established that Aβ monomers form micelle-like structures above a critical concentration, $c^* \approx 100$ μM (8). Nuclei arise from these micelles, and fibrils grow from nuclei through the addition of Aβ monomers to the fibril ends. This fibrillogenesis mechanism is supported by the data presented in Fig. 1. This figure shows the time evolution of the size distribution of the scattering particles in a 250 μM Aβ solution. Immediately on dissolution, the major contribution to the light scattering comes from particles with hydrodynamic radii of $\approx$7 nm (Fig. 1*A*). These particles are never observed at Aβ concentrations below c^*. This fact, together with the known amphiphilic potential of Aβ monomer (21) and a theoretical analysis of the kinetics of Aβ fibrillogenesis (8), is consistent with the 7-nm peak in Fig. 1 representing micelle-like aggregates of Aβ monomers. Over time, a new peak emerges (Fig. 1 *B–F*). The average R_h for this peak is bigger than that of the micelles and increases with time. The intensity of the scattered light also increases and is nearly proportional to the size of the scattering particles (data not shown). The proportionality between average size and intensity of scattering is indicative of one-dimensional (fibrillar) growth of the scattering objects. We therefore ascribe this distribution to mature

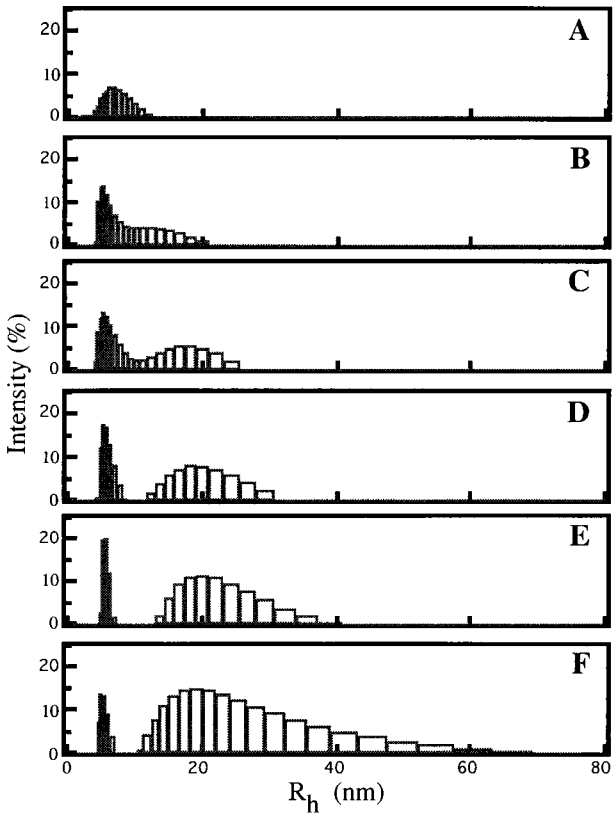

FIG. 1. Temporal evolution of the size distribution of the scattering particles in a 250 μM Aβ solution. (*A*) One hour after sample preparation. The major contribution to scattering comes from micelle-like aggregates of Aβ monomers with $R_h \approx 7$ nm. (*B–F*) Scattering 1.5 hr (*B*), 2 hr (*C*), 3 hr (*D*), 4 hr (*E*), 6 hr (*F*) after sample preparation. A second distribution, with an average R_h larger than 7 nm, emerges from the micellar distribution and grows in size over time. This second distribution is produced by mature Aβ fibrils.

Aβ fibrils. Indeed, electron microscopy and circular dichroism experiments performed on equivalent samples reveal fibrils with quaternary and secondary structures indistinguishable from those observed in fibrils from plaques (8).

After 4 hr of incubation, when fibrils reached $R_h \approx 20$ nm, a sample was diluted to 50 μM, divided into four aliquots, and further fibril growth was monitored at 4°C, 15°C, 25°C, and 35°C. We found that the elongation rates vary dramatically with temperature. Fig. 2 displays on a logarithmic scale the initial elongation rates dN_f/dt as a function of inverse temperature. These data points could be fit well with a straight line. According to Eq. **1**, the elongation rate is $k_e c$, where the concentration of monomers c is a temperature-independent quantity. Therefore, the elongation rate constant follows the Arrhenius law:

$$k_e = A \exp(-E_A/RT). \qquad [2]$$

The slope of the straight line in Fig. 2 determines the activation energy E_A, which was calculated to be 22.8 ± 1.1 kcal/mol (1 kcal = 4.18 kJ). Measurements represented in this figure were performed on the preincubated samples with identical starting concentrations of Aβ and identical number concentrations of fibrils. Moreover, after dilution, the only process that occurs in these samples is the elongation of fibrils, with the rate dependent on the temperature. Thus, the curves for the time evolution of the apparent hydrodynamic radius differ only in the scale of time which is set by k_e. However, a more accurate determination of the elongation rate constant requires measurements of the size evolution of shorter fibrils at the initial stage of the fibrillogenesis process, since for

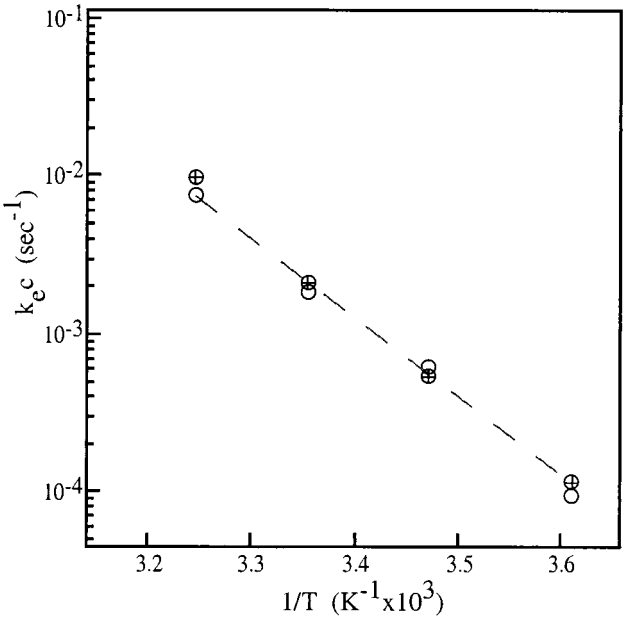

FIG. 2. Arrhenius plot of initial elongation rate vs. inverse temperature for 50 μM samples. Two sets of samples (◯, ⊕) were prepared under controlled nucleation conditions. The resulting data could be fit well with a straight line ($R = -0.99$), whose slope yielded an activation energy, E_A, of 22.8 ± 1.1 kcal/mol.

shorter fibrils the relative increase in the fibril length is much more pronounced. Also, entanglement of longer fibrils modifies their diffusion. This leads to a systematic overestimation of the length of the fibrils as determined from QLS data. At the same mass concentration of fibrils, this type of error is much less significant for short fibrils than for long ones.

In Fig. 3, we show the temporal evolution of the mean hydrodynamic radius of Aβ fibrils incubated at two different temperatures immediately upon dissolution. The nominal concentration of Aβ was 250 μM and the measurements were taken at 24°C (+) and 4°C (◯). We see from the initial slopes of the curves that the elongation rate increased dramatically

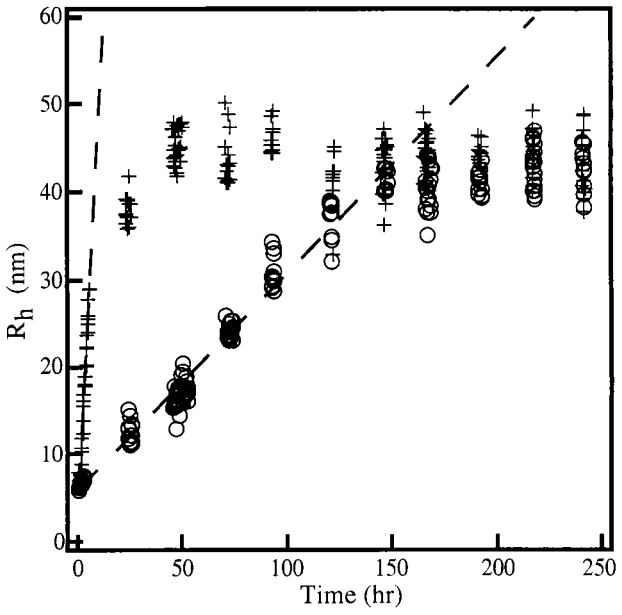

FIG. 3. Temporal evolution of the mean hydrodynamic radius R_h of Aβ fibrils. Samples of Aβ at 250 μM concentration were incubated at 24°C (+) or 4°C (◯). Slopes of dashed lines indicate initial elongation rates at each temperature.

with temperature. By using the interpolation formula relating the average hydrodynamic radius R_h to fibril length L (8), the elongation rates were calculated to be 18.6 nm/hr for 24°C and 1.0 nm/hr for 4°C. An increase in the temperature by 20°C results in an increase in the elongation rate by a factor of 20. Although the two samples used for these measurements came from the same initial solution, it was possible that identical numbers of fibrils would not be nucleated in each, because these two samples were kept at different temperatures and the nucleation rate could be temperature-dependent. However, as seen in Fig. 3, the final size of fibrils was similar at both temperatures. Because the total concentration of peptide was the same, this indicates that approximately equal numbers of fibrils were, in fact, nucleated in each sample. The activation energy determined from these measurements yielded the same value as the less accurate procedure using controlled nucleation (Fig. 2). Clearly, our measurement of the elongation rate is insensitive to the nucleation step of the fibrillogenesis process. This is expected because the QLS method measures the length of individual fibrils. The results of such measurements are insensitive to variations in the number concentration of fibrils, assuming noninteracting particles.

In Fig. 4, we summarize all our data in a semilogarithmic plot of the initial elongation rates of Aβ fibrils. The dashed line is a linear fit to the 50 μM sample data from Fig. 2. Measurements carried out concurrently at two different temperatures for Aβ samples of concentration 100 μM (△, ▽), 125 μM (◊), 250 μM (◇), and 375 μM (□) all yielded approximately the same value for the activation energy, E_A = 23.0 ± 0.6 kcal/mol. This coincided, within the statistical error, with the value found for the samples with controlled nucleation. Note that the last three nominal concentrations are above c^*. At concentrations of soluble Aβ above the critical concentration, the concentration of free monomers is effectively fixed at c^* and the elongation rate should therefore be $k_e c^*$ (8, 19). The identical slopes of the Arrhenius plots determined above and below c^* indicate that this critical micellar concentration is independent of the temperature, within our experimental error. Taking $c^* = 100$ μM, the value of the preexponential factor A in Eq. **2** is $\approx 6 \times 10^{18}$ liter/(mol · sec).

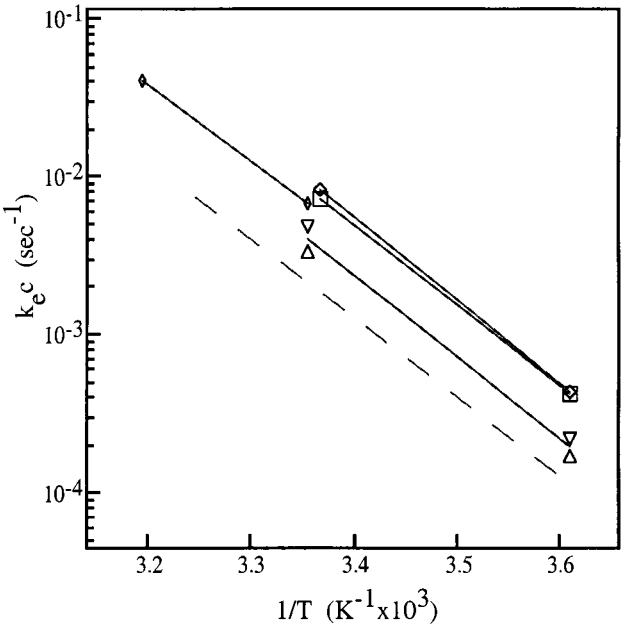

FIG. 4. Arrhenius plot of elongation rates as a function of inverse temperature. Nominal Aβ concentrations are 100 μM (△, ▽), 125 μM (◊), 250 μM (◇), and 375 μM (□). The dashed line is the linear fit of the data for the 50 μM samples presented in Fig. 2. Samples with nominal concentrations of 125 and 100 μM, which are only slightly above c^*, actually showed elongation rates of approximately 0.8 and 0.4, respectively, of the maximal value $k_e c^*$. Clearly, in the process of preparation, the concentrations of soluble Aβ were reduced in the 125 μM sample to $0.8c^*$ (centrifugation) and in the 100 μM sample to $0.4c^*$ (filtration). Furthermore, the estimated concentration of free monomers in the preincubated sample immediately after dilution was 25 μM (Fig. 2; ○, ⊕). This value is consistent with the fact that fibrils of about half the expected final length were formed, suggesting that approximately half of the initial 250 μM concentration of free monomers was consumed before the 5-fold dilution of the sample.

We may analyze the above results in the framework of the transition state theory for the rate of chemical reaction between free Aβ monomer and fibril end (22). We assume that the monomer can bind to the fibril tip only when it is inside the reaction volume v with the characteristic size $l \approx v^{1/3}$. We also assume that the monomers entering the reaction volume can actually bind to a fibril only if these monomers or the fibril tip (or both) are in the appropriate activation state. The probability of the occurrence of such a state is $\exp(-\Delta G/kT)$, where ΔG is the change in free energy associated with the activation process. Thus the rate of fibrillar growth can be written as

$$\frac{dN_f}{dt} = \Gamma \exp(-\Delta G/RT), \qquad [3]$$

where Γ is the number of monomers entering the reaction volume per unit time. To estimate Γ, we note that the rate with which monomers enter a certain volume is equal to the rate with which they leave this same volume. The average number of monomers in a volume v at any moment of time is cv. These monomers are in a constant Brownian motion and diffuse out of this volume in a time $\tau \approx l^2/D \approx v^{2/3}/D$, to be replaced by others. Thus the number of monomers entering the reaction volume per unit time is cv/τ, and therefore

$$\Gamma \cong cv^{1/3}D. \qquad [4]$$

It is reasonable to assume that the size of the reaction volume is of the order of the size of a monomer. Note that in this case the magnitude of the "encounter time" τ becomes comparable to the characteristic time constant for the monomer reorientation, i.e., to the reciprocial of the monomer rotational diffusion coefficient. Implicit in our derivation of Eq. **3** is the assumption that the "encounter time" τ that the monomer spends within the reaction volume is short compared to the lifetime τ_A of an activated state. If this were not the case, the possibility of activation during the encounter would need to be taken into account. We shall justify the assumption $\tau \ll \tau_A$ later.

Substituting Eq. **4** into Eq. **3**, using the thermodynamic relationship $\Delta G = E_A - T\Delta S$, where ΔS is the change in the entropy associated with the activation process, and comparing with Eq. **1**, we have

$$k_e = v^{1/3}D \exp(\Delta S/R) \exp(-E_A/RT). \qquad [5]$$

Eq. **5** permits a physicochemical interpretation of the significance of the parameters A and E_A, as obtained from the experimental measurements of $k_e(T)$ (Eq. **2**). One can see from comparison of Eq. **5** and Eq. **2** that the activation entropy ΔS is related to the parameter A by

$$\Delta S = R \ln\left(\frac{A}{v^{1/3}D}\right). \qquad [6]$$

In this equation, the diffusion coefficient of the free monomer, D, is 1.6×10^{-7} cm$^2 \cdot$ sec^{-1} (for R_h = 1.8 nm (11)). Because of the uncertainty in the initial concentration of free Aβ monomers and the value of c^*, the quantity $A \approx 6 \times 10^{18}$ liter/(mol·sec) is known only within a factor of 2. The reaction volume size $\ell = v^{1/3}$ is also not well known. We

may take it to be of the order of the dimension of the Aβ monomer, namely ≈ 1 nm. Using these values in Eq. **6** provides $\Delta S = 5.3 \times 10^{-2}$ kcal/(K·mol) or $T\Delta S = 16$ kcal/mol at 300 K. Although the values used to calculate the activation entropy are not known accurately, even a factor of 10 uncertainty in the magnitude of $A/v^{1/3}$ introduces an error of only $2.3RT = 1.4$ kcal/mol in $T\Delta S$, which is less then 10% of the total value of ≈ 16 kcal/mol. Note that, in comparison with the uncertainty in $v^{1/3}$, the error in the numerical value of A caused by a poorly known monomer concentration c produces an insignificant effect on the deduced value of the activation entropy ΔS.

The change in free energy associated with the activation process, $\Delta G = E_A - T\Delta S = 7$ kcal/mol, is a relatively small quantity, so the probability of an activated state occurring, $\exp(-\Delta G/RT) \approx 10^{-5}$, is sufficiently large for the reaction to occur at the observed rate. However, this small free energy results from the difference between the much larger activation energy $E_A = 23.0$ kcal/mol and the entropy contribution, $T\Delta S = 16$ kcal/mol (at 300 K). The activated and inactive states differ significantly in both energy and entropy, suggesting a substantial difference in structure. Several factors may contribute to the increased entropy of the activated state, including unfolding of protein and release of bound water molecules. Since activation is also accompanied by a significant increase in energy, it is likely that a transition from a more ordered, bound structure to a more disordered, loose structure is the essence of the activation process preceding monomer binding to a growing fibril.

It is illuminating to compare the thermodynamics of Aβ activation with that of conformational change of peptides of similar size. In Table 1, we present the values of E_A, $T\Delta S$, and ΔG, as determined in the present paper for Aβ, and those for the unfolding (melting) of several peptides with known secondary structures. These include chymotrypsin inhibitor 2 (23), the N-terminal domain (λ_{6-85}) of phage λ repressor (24, 25), the SH3 domain of spectrin (26), and the C-terminal fragment (41–56) from protein GB1 (27). Table 1 shows that the thermodynamic parameters of Aβ activation are of the magnitude expected for conformational rearrangment of a peptide of this size. A key question is where this rearrangment occurs, i.e., in the soluble monomer, at the fibril tip, or in both. Recent studies (28) indicate that soluble Aβ monomer may not possess a stable structure which could "unfold" in the activation process. On the other hand, amyloid fibrils do have a stable structural organization (5). It is therefore conceptually attractive to envision a partial unfolding of the organized fibril end to accommodate addition of an incoming Aβ monomer. This process would involve bond breaking among Aβ monomers constituting the fibril tip with its obligatory activation energy, partial unfolding of these molecules with a resultant increase in entropy, and subsequent bond reformation and entropic loss concurrent with incorporation of the new, incoming Aβ molecule.

We now examine numerically the validity of our assumption that $\tau \ll \tau_A$. Using the values of D and l established above, we estimate the encounter time $\tau = l^2/D \approx 70$ ns. We expect this time to be small compared to the "lifetime" of the activated "unfolded" state. [Note that the lifetime of the inactive state is $\exp(\Delta G/RT) \approx 10^5$ longer than the activated one.] For comparison, the time constant associated with the kinetics of β-hairpin formation for the GB1 protein fragment (27) listed in Table 1 is 3.7 μsec. This time is more than an order of magnitude larger than the estimated encounter time between an Aβ monomer and a fibril tip. The GB1 protein fragment is small compared to Aβ and even more so compared to the fibril tip. For larger peptides, the kinetics of folding slows down dramatically. For instance, the time constant for λ_{6-85} folding is about 300 μsec (24). These comparisons justify our assumption that the encounter between Aβ monomer and fibril tip is so short that the possibility of transitions between active and inactive conformations during this moment can be ignored.

Table 1. Thermodynamic parameters for small peptides

Peptide	No. of residues	E_A (ΔH)	$T\Delta S$	ΔG	Structure
Aβ	40	23.0 ± 0.6	≈ 16	≈ 7	?
CI2 (23)	64	31.2	24.6	6.5	α/β
λ repressor (24, 25)	80	16.1 ± 0.1	12.8	3.3	α
SH3 (26)	62	9.5	6.5	3.0	β
GB1(41–56) (27)	16	11.6	11.7	0.1	β-hairpin

E_A, $T\Delta S$, and $\Delta G \equiv E_A - T\Delta S$ are in kcal/mol. $T = 300$ K for all peptides except for λ repressor, which was studied at 37°C (310 K).

A significant conformational change is required for a binding reaction to occur. The probability of this change, $\exp(-\Delta G/RT)$, is a key factor in determining the Aβ fibril elongation rate constant k_e. A natural deduction from this fact is that chemical interventions that stabilize the inactive state of soluble Aβ monomer or fibril tip can have a very profound effect on the rate of Aβ fibrillogenesis. To increase ΔG, these interventions should either lower the energy of the inactive state of Aβ or decrease the entropy of the activated, unfolded state, or both. One can also envision strategies targeting the growing fibril tip. A simple example is competitive inhibition by a ligand that can block fibril elongation by binding to the fibril tip. If the equilibrium dissociation constant K is very small, even a moderate concentration of the ligand, C_L, will "poison" the growing tip of the fibril and reduce the elongation rate by the factor K/C_L. This factor is simply the probability that the fibril tip is free of a ligand molecule, provided $C_L \gg K$. Within the framework of our analysis, the effect of such a ligand can be described as an increase in the activation free energy ΔG by the quantity $RT \ln(C_L/K)$, which is essentially the free energy needed to remove the ligand from the fibril tip.

CONCLUSIONS

Using QLS spectroscopy, we studied the fibrillogenesis of Aβ(1–40) in 0.1 M HCl solution and measured, as a function of temperature, the rate constant k_e for Aβ fibril elongation. Within the temperature range 4–40°C, we have found that the elongation rate varies over two orders of magnitude and obeys the Arrhenius law. The activation energy of the reaction, $E_A = 23$ kcal/mol, indicates that Aβ monomer binding to fibril tip proceeds via an activated state. Accordingly, we have used transition state theory for reaction kinetics to estimate the entropy change associated with the transition into the activated state. This theory assumes that the lifetime of the activated state is much longer than the encounter time between monomer and fibril tip. We have deduced that the activation process involves a very significant increase in entropy, $T\Delta S \approx 16$ kcal/mol at 300 K. These values for E_A and ΔS are consistent with the notion that the activation process involves unfolding of Aβ within the growing fibril tip, of soluble Aβ, or both.

The magnitude of the dependence of the elongation rate constant on the free energy of activation clearly indicates that the activation step in binding of monomer to fibril end is a prime target for therapeutic inhibitors of fibril growth. Indeed, agents that increase the energy required for activation or decrease the entropy in the activated state should produce a profound reduction in the elongation rate. The present findings indicate that theoretical analysis of measurements of the magnitude and temperature dependence of fibril elongation rates can provide valuable insights into the process of monomer addition at the growing fibril tip. Furthermore, our results demonstrate that experimental methodology based on the QLS method can serve as a powerful quantitative assay to test the efficacy of putative inhibitors of Aβ fibril growth.

Ms. Jennifer Nickel made initial measurements at the early stage of this project. We thank Drs. Felix Villars, William Eaton, and Peter Lansbury for useful critical comments, Drs. Dominic Walsh and Youcef Fezoui for numerous helpful discussions, and Ms. Margaret Condron for expert technical assistance. This work was supported by National Institutes of Health Grant 1P01AG14366 (G.B.B. and D.B.T.), by the Foundation for Neurologic Diseases (D.B.T), and by Amgen/Massachusetts Institute of Technology and Amgen/Brigham and Women's Hospital Research Collaboration Agreements (G.B.B and D.B.T.).

1. Iqbal, K. (1991) in *Alzheimer's Disease: Basic Mechanisms, Diagnosis, and Therapeutic Strategies,* eds. Iqbal, K., McLachlan, D. R. C., Winblad, B. & Winsniewski, H. M. (Wiley, New York), pp. 1–5.
2. Selkoe, D. J. (1991) *Neuron* **6,** 487–498.
3. Yankner, B. A. (1996) *Neuron* **16,** 921–932.
4. Selkoe, D. J. (1996) *J. Biol. Chem.* **271,** 18295–18298.
5. Selkoe, D. J. (1994) *J. Neuropathol. Exp. Neurol.* **53,** 438–447.
6. Hardy, J. (1997) *Trends Neurosci.* **20,** 154–159.
7. Jarrett, J. T. & Lansbury, P. T., Jr. (1993) *Cell* **73,** 1055–1058.
8. Lomakin, A., Chung, D. S., Benedek, G. B., Kirschner, D. A. & Teplow, D. B. (1996) *Proc. Natl. Acad. Sci. USA* **93,** 1125–1129.
9. Naiki, H. & Nakakuki, K. (1996) *Lab. Invest.* **74,** 374–383.
10. Esler, W. P., Stimson, E. R., Ghilardi, J. R., Vinters, H. V., Lee, J. P., Mantyh, P. W. & Maggio, J. E. (1996) *Biochemistry* **35,** 749–757.
11. Walsh, D. M., Lomakin, A., Benedek, G. B. & Teplow, D. B. (1997) *J. Biol. Chem.* **272,** 22364–22372.
12. Garzon-Rodriguez, W., Sepulveda-Becerra, M., Milton, S. & Glabe, C. G. (1997) *J. Biol. Chem.* **272,** 21037–21044.
13. Andreu, J. M. & Timasheff, S. N. (1986) *Methods Enzymol.* **130,** 47–59.
14. Jarrett, J. T., Berger, E. P. & Lansbury, P. T., Jr. (1993) *Biochemistry* **32,** 4693–4697.
15. Naiki, H., Gejyo, F. & Nakakuki, K. (1997) *Biochemistry* **36,** 6243–6250.
16. Cohen, R. J. & Benedek, G. B. (1975) *Immunochemistry* **12,** 349–351.
17. Tomski, S. J. & Murphy, R. M. (1992) *Arch. Biochem. Biophys.* **294,** 630–638.
18. Shen, C. L. & Murphy, R. M. (1995) *Biophys. J.* **69,** 640–651.
19. Lomakin, A., Teplow, D. B., Kirschner, D. A. & Benedek, G. B. (1997) *Proc. Natl. Acad. Sci. USA* **94,** 7942–7947.
20. Braginskaya, T. G., Dobitchin, P. D., Ivanova, M. A., Klyubin, V. V., Lomakin, A. V., Noskin, V. A., Shmelev, G. E. & Tolpina, S. P. (1983) *Phys. Scr.* **28,** 73–79.
21. Soreghan, B., Kosmoski, J. & Glabe, C. (1994) *J. Biol. Chem.* **269,** 28551–28554.
22. Eisenberg, D. & Crothers, D. (1979) *Physical Chemistry* (Benjamin/Cummings, Menlo Park, CA), pp. 242–244.
23. Jackson, S. E. & Fersht, A. R. (1991) *Biochemistry* **30,** 10428–10435.
24. Huang, G. S. & Oas, T. G. (1995) *Proc. Natl. Acad. Sci. USA* **92,** 6878–6882.
25. Scalley, M. L., Yi, Q., Gu, H., McCormack, A., Yates, J. R., III, & Baker, D. (1997) *Biochemistry* **36,** 3373–3382.
26. Viguera, A. R., Martinez, J. C., Filimonov, V. V., Mateo, P. L. & Serrano, L. (1994) *Biochemistry* **33,** 2142–2150.
27. Muñoz, V., Thompson, P. A., Hofrichter, J. & Eaton, W. A. (1997) *Nature (London)* **390,** 196–199.
28. Teplow, D. B. (1998) *Amyloid* **5,** 121–142.